UC Davis
UC Davis Previously Published Works

Title
Retinal topography maps in R: New tools for the analysis and visualization of spatial retinal data

Permalink
https://escholarship.org/uc/item/927624pg

Journal
Journal of Vision, 15(9)

ISSN
1534-7362

Authors

Cohn, Brian A
Collin, Shaun P
Wainwright, Peter C
et al.

Publication Date
2015-07-31

DOI
10.1167/15.9.19

Peer reviewed

Retinal topography maps in R: New tools for the analysis and visualization of spatial retinal data

Brian A. Cohn

W.M. Keck Science Department, Claremont McKenna, Pitzer, and Scripps Colleges, Claremont, CA, USA

Shaun P. Collin

School of Animal Biology and the Oceans Institute, The University of Western Australia, Crawley, Perth, Western Australia, Australia

Peter C. Wainwright

Department of Evolution and Ecology, University of California Davis, Davis, CA, USA

Lars Schmitz

W.M. Keck Science Department, Claremont McKenna, Pitzer, and Scripps Colleges, Claremont, CA, USA

Retinal topography maps are a widely used tool in vision science, neuroscience, and visual ecology, providing an informative visualization of the spatial distribution of cell densities across the retinal hemisphere. Here, we introduce Retina, an R package for computational mapping, inspection of topographic model fits, and generation of average maps. Functions in Retina take cell count data obtained from retinal wholemounts using stereology software. Accurate visualizations and comparisons between different eyes have been difficult in the past, because of deformation and incisions of retinal wholemounts. We account for these issues by incorporation of the R package Retistruct, which results in a retrodeformation of the wholemount into a hemispherical shape, similar to the original eyecup. The maps are generated by thin plate splines, after the data were transformed into a two-dimensional space with an azimuthal equidistant plot projection. Retina users can compute retinal topography maps independent of stereology software choice and assess model fits with a variety of diagnostic plots. Functionality of Retina also includes species average maps, an essential feature for interspecific analyses. The Retina package will facilitate rigorous comparative studies in visual ecology by providing a robust quantitative approach to generate retinal topography maps.

Introduction

As a "window" into the brain, the retina provides insights into the visual requirements of an animal within its ecological niche. A wide variety of studies on vertebrate visual ecology have explored how its evolution is correlated with each species' visual environment. An effective way to study the morphological diversity of the retina is the *wholemount* technique. Retinal wholemounts provide easy access to neuronal structures from both the vitread and sclerad sides of the retina, which have already led to remarkable discoveries in the 19th century (e.g., Chievitz 1889). Stone (1981) has also provided a comprehensive overview of retinal whole-mounting, a technique that remains important to this day (e.g., Fileta et al., 2008; Ullmann, Moore, Temple, Fernández-Jurecic, & Collin, 2012). The preparation of the wholemount involves making small radial incisions in the eyecup, removing the underlying retinal pigment epithelium, and unfolding the extracted retina. Cells of the retina are stained, surveyed under a microscope, and analyzed from a physiological, functional, and ecological perspective. For example, retinal ganglion cells (RGC) line the retina and sum the signals from photoreceptors in the vertebrate eye (Shapley & Perry, 1986) and set the limits of spatial resolving power, where behavioral limits of acuity have been found to match anatomical estimates (Temple, Manietta, & Collin, 2013). Comparative biologists often measure
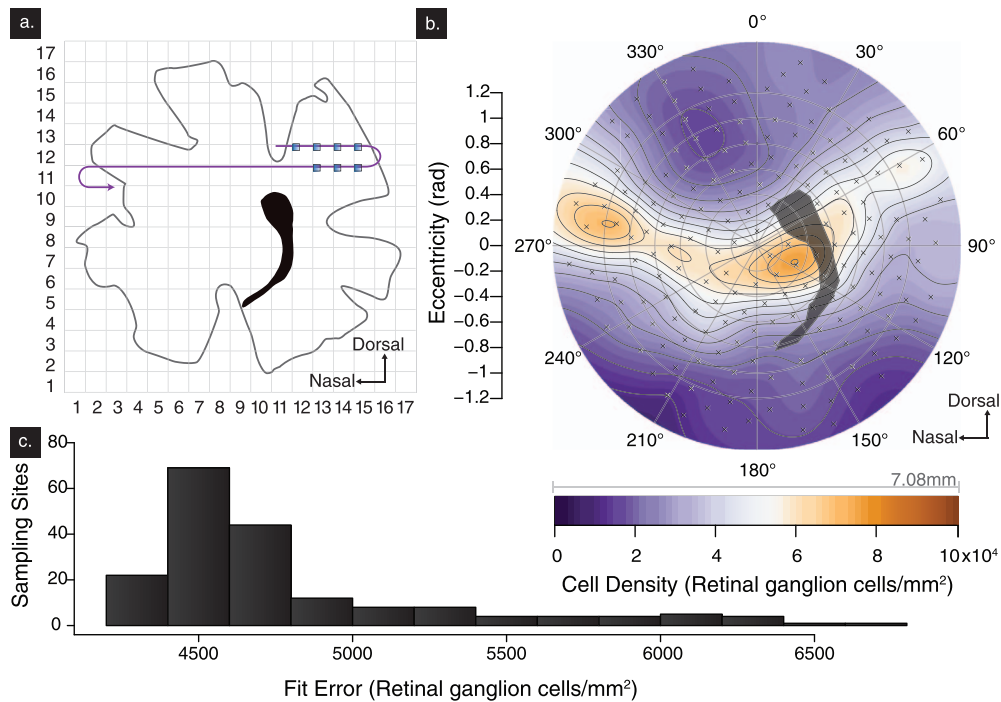
Figure 1. The R package Retina facilitates visualization of cell count data obtained from retinal wholemounts. (A) Simplified retinal wholemount with superimposed stereology sampling grid. The sampling locations are at the intersections of the uniform grid. (B) Retinal topography map of the labrid reef fish *Novaculichthys taeniourus*. The map is oriented so that nasal is to the left, and dorsal on top. The smoothing parameter was set to $\lambda = 0.001$, combined with a second order polynomial. (C) Frequency distributions of model error (difference between true and predicted cell density) at each sampling location.

the peak density of cells in the ganglion cell layer to understand the upper limit of visual acuity (Collin & Pettigrew, 1989), and analyze the spatial distribution of cells across the retinal hemisphere to provide a map of estimated visual performance across different regions of an animal's visual space (Collin, 2008). Cell densities have been traditionally visualized as *retinal cell topographies*, an isodensity surface plot within a wholemount outline. In the 19th century, retinal topography maps were mentioned by von Graefe (1865, p. 22, "Netzhautkarte") and, to our best knowledge, were formally introduced by Stone (1965). Retinal topography maps have since been widely used, with many recent publications (e.g., Ahnelt, Schubert, Kübber-Heiss, Schiviz, & Anger, 2006; Coimbra, Nolan, Collin, & Hart, 2012; Coimbra, Collin, & Hart, 2013, 2014a, 2014b; Landgren, Fritsches, Brill, & Warrant, 2014; Lisney, T. J., Stecyk, K., Kolominsky, J., Graves et al., 2013; Lisney, T. J., Stecyk, K., Kolominsky, J., Schmidt et al., 2013; Moore, Doppler, Young, & Fernandez-Juricic, 2013; Newman, Marshall, & Collin, 2013; Schiviz, Ruf, Kuebber-Heiss, Schubert, & Ahnelt, 2008; Ullmann et al., 2012). Comparative analyses over the last few decades have yielded maps for several hundred vertebrates, many of which (approx. 191) are available in an online database (Collin, 2008).

Retinal maps are often generated from cell counts measured across a regular sampling grid, using a variety of commercial stereology software solutions (Ullmann et al., 2012). Such a systematic random sampling approach is considered more efficient and less prone to bias than other sampling techniques (West, 2012). Sampling locations, usually about 200 per retina, are at the intersections of the gridlines (Figure 1A). Regardless of cell type, their distributions have been difficult to compare between eyes for various reasons. First, the location of the peripheral slits made to wholemount the retina and construct the topography map are not consistent. Deformed wholemounts have varying shapes according to where the incisions have been made, which, in most cases, makes it difficult to orient multiple retinas. Second, there are currently no tools specifically tailored to the smoothing of retinal data that is necessary for generating the maps. Contour lines are often drawn by hand, or require commercial mapping or geographic information systems (GIS) software to perform the interpolation (e.g., Ahnelt et al., 2006; Lisney, T. J., Stecyk, K., Kolominsky, J., Graves et al., 2013; Lisney, T. J., Stecyk, K., Kolominsky, J., Schmidt et al., 2013). While the application of GIS methods to retinal map generation is a big step toward a more quantitative analysis, the proprietary nature of the software prevents wide

distribution and user customization of underlying algorithms.

Substantial advances in retinal topography visualization resulted from Curcio, Sloan, and Meyers (1989), with retinal reconstruction from a flat mount and subsequent smoothing of density data following projection of the hemisphere onto an azimuthal equidistant polar projection. This approach also introduced a common coordinate system among retinas of different sizes, using eccentricity from the axial pole and longitude to define a position on a human retina. Mass and Supin (1989) also introduced innovative approaches to correct angular distortion of retinal wholemounts, yet did not fully elaborate the details of their method. Mathematical procedures were not fully described until later (Chelvanayagam, 2000). Even though each of the above-mentioned studies outlines promising pathways to potentially more rigorous generation of retinal topography maps, vision scientists still often prefer the traditional approach.

An important milestone in tool development was reached recently. A freely available R (R Development Core Team, 2014) package, Retistruct, is now available for the reconstruction of the hemispherical nature of the eye from the retinal wholemount (Sterratt, Lyngholm, Willshaw, & Thompson, 2013). New insights on the effects of smoothing and visualization of retinal data have also come to light recently (Garza-Gisholt, Hemmi, Hart, & Collin, 2014). Garza-Gisholt and colleagues demonstrated that several smoothing and interpolation techniques resulted in similar retinal topography maps, but noted that the thin plate spline models can produce smoother appearances.

In order to facilitate new pathways to the visualization of retinal topography data, we developed a new tool that combines Retistruct (Sterratt et al., 2013) with the recently gained knowledge about computational mapping of retinal topography (Garza-Gisholt et al., 2014). We also added utility functions that allow for inspection of topographic model fits and the generation of average maps from several individuals of a species. With the R package Retina, we provide free, open source software that represents a novel tool for the visualization of cell densities across retinal wholemounts of chambered eyes.

Required software

We developed Retina in R, version 3.1.3, a free language for statistical computing (R Development Core Team, 2014). A freely available image editor, ImageJ 1.47v (Abràmoff, Magalhães, & Ram, 2004), must be also installed for steps in data preparation. The workflow was developed and tested on Mac OSX 10.10.12, Windows 7 Enterprise, Windows 8.1 (x86, x64, and ARM), and Ubuntu (12.04 LTS and 14.04). Currently, Retina is readily available on GitHub (http://github.com/bcohn12/retina and http://github.com/lschmitz/retina) and will also be submitted to the Comprehensive R Archive Network (CRAN).

Data acquisition

In order to illustrate the functionality of Retina, we collected data on two teleost fishes, the chiseltooth wrasse *Pseudodax moluccanus* (Labridae) and the rockmover wrasse *Novaculichthys taeniourus* (Labridae). Animal use was in adherence to the ARVO Statement for the Use of Animals in Ophthalmic and Vision Research. All specimens of the chiseltooth wrasse, *P. moluccanus*, were purchased from local commercial suppliers in Perth, Western Australia. All procedures closely followed the ethical guidelines of the National Health and Medical Research Council of Australia approved by The University of Western Australia Animal Ethics Committee (AEC Permit RA/3/100/917). The specimen of the rockmover wrasse, *N. taeniourus*, was acquired from the pet trade in California and handled according to the UC Davis IACUC protocol. Retinas were fixed in 4% paraformaldehyde in 0.1M phosphate buffer and wholemounted following standard procedures (Ullmann et al. 2012). After Nissl staining, the samples were surveyed with an Olympus BX50 microscope (Olympus, Tokyo, Japan) equipped with a motorized stage, using the optical fractionator module of Stereo Investigator (MBF Bioscience, Williston, VT). Cell densities represent the total number of cells in the retinal ganglion cell layer (retinal ganglion cells and amacrine cells but not glial cells). For all samples, we surveyed about 200 sites (*N. taeniourus*, 206; *P. moluccanus*, 197 and 205 sites, respectively). The sampling for *N. taeniourus* was set to 320×320 μm, and to 452×542 μm and 390×397 μm for the two retinal wholemounts of *P. moluccanus*. The counting frame size was 25×25 μm for all sampling sites and all specimens. All count data and stereology parameters are included as example files in the Retina package, and will also be available on DRYAD digital repository. To access parameters and data, type Pmol_752, Pmol_753, or Ntae_381 in the R command line after loading Retina.

Outline of the Retina workflow

The following sections provide an overview of the functionality of Retina. For detailed instructions, please refer to our installation guide, a step-by-step user tutorial, and an overview readme file available in the Supplementary Information. By default, Retina

assumes a uniform sampling grid, which is considered to minimize possible bias in reconstructing distribution of cells (West, 2012). If counts from nonuniform sampling grids are available, one can still use Retina, but should follow a slightly different procedure that is briefly outlined in the step-by-step user tutorial. Please note that we recommend the use of data from uniform sampling grids, following standard procedures from stereology (Ullmann et al., 2012; West, 2012).

Initial data input

After using stereology software to measure cell counts (z) at each sampling location, an image (screenshot) of the retinal outline beneath a sampling grid (Figure 1A) is used to manually assign unique column (x) and row (y) indices to each count (z). This yields a three-column dataset with count (z) at given (x, y) locations. Sampling locations outside the retinal outline are set as not applicable (NA).

Data preparation in ImageJ

The goal of this step is to convert the (x, y, z) grid data, and the retinal region of interest (ROI) into pixel units compatible with Retina. Stereology software stores sampling locations in a variety of formats; adding this extra step with ImageJ enables wide application across different stereology systems. Although ImageJ has facilities for specifying the units of distance across an image in millimeters (among other measurement methods), Retina does not require units for its reconstruction. We exclude this additional step of calibration to reduce the amount of time required to complete data preparation, but calibrated units work equally well with our program, as long as unit-calibrated coordinates are consistent between the region of interest and the falciform process/optic disk.

The screenshot of the retinal outline and sampling locations is loaded into ImageJ, and the pixel coordinates of sampling locations at the far edges of the sampling grid (far-left, far-right, top-most, bottom-most) are recorded. Pixel coordinates of all sampling locations are calculated on the basis of column and row numbers, knowing that the sampling grid is uniform. ImageJ is then used to obtain the outline of the entire retina with the polygon selection tool. The traced outline is saved via the ROI manager. The polygon tool is also used to outline the position of the optic nerve head (and falciform process, if present), which are saved as (x, y) coordinates.

Data transformation in Retina (using Retistruct)

The next step is carried out with the Retina package for R. Once the coordinates for sampling locations and the retinal outline are prepared, the deformation of the retina caused by the incisions and subsequent flattening can be corrected with Retistruct (Sterratt et al., 2013). For details of the Retistruct approach please refer to Sterratt et al. (2013). Here we provide some basic elements that are directly relevant for successful retinal topography map computation. The Retistruct package is invoked with the command retistruct(), and the user can then manually markup the retinal folds based on the outline and carefully identify the anatomically correct orientation of the sample. Within the Retistruct graphical user interface, each incision is marked at the deepest point of the cut, and at the two peripheral points at the retina's peripheral rim (Sterratt et al., 2013; Supplementary Information). We wrote the wrapper function retina_object(), which utilizes both the stereology and Retistruct data, and outputs spherical coordinates (latitude, longitude) of each sampling location. The outline of the optic nerve head and the falciform process (if present) are also provided as spherical coordinates. A plot of the reconstructed data points on an interactive sphere is generated to assess if data transformation was carried out correctly. As long as the sampling sites were uniformly distributed across the entire wholemount, the coordinates for the cell counts will be distributed across the surface of only the lower hemisphere. As we model the retina as a hemisphere, with the axial pole directed posteriorly, no cell counts should appear above the equator; points on the anterior side of the sphere indicate errors in the data preparation stage.

Polar projection, model fitting, and plotting in Retina

This is carried out with the retinaplot() function, which combines several computational procedures into one single step; a brief description of our approach follows below.

We transform the spherical coordinates to two-dimensional space with an azimuthal equidistant plot projection, which displays the entire retinal hemisphere as a true directional projection for plotting (Borodkin & Thompson, 1992; Snyder, 1987). Azimuthal equidistant projections are widely used in cartography (Bugayevskiy & Snyder, 2002) and have also been applied to human perimetry (Frisén, 1970) and retinal mapping (Curcio et al., 1989). Distances along the lines extending radially from the retina's center are equal to the retina's great circle distance. Polar angles are represented exactly, and latitudinal lines are presented with equal distance between one another (Snyder,
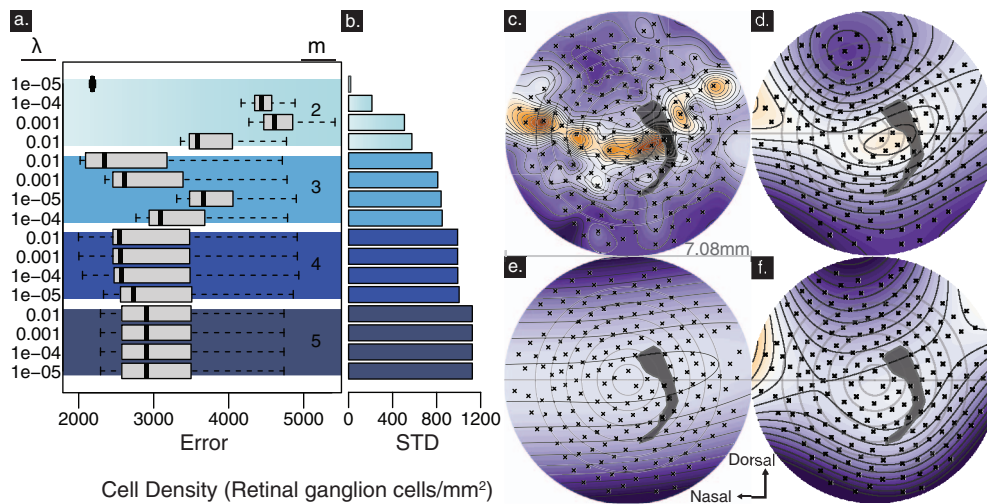
Figure 2. Smoothing parameter settings (λ; m = polynomial order) of thin plate splines showing the effects on the appearance of retinal cell topography maps (rockmover wrasse, *N. taeniourus*). Small standard deviations of the errors reveal that overall the topography is traced reasonably well, even though the mean error may be larger than in other maps (A, B; note that outliers were removed for clarity). However, smaller predicted errors often occur in maps that are overly complex (C, $\lambda = 0.00001$ and $m = 2$) or overly smooth (D, $\lambda = 0.01$ and $m = 3$; E, $\lambda = 0.0001$ and $m = 3$; F, $\lambda = 0.001$ and $m = 4$). In all maps, nasal is to the left, and dorsal towards the top.

1987). The azimuthal equidistant projection has higher scale distortion (width exaggeration) toward the retinal periphery. While other map projection options distort the central region of the retina (i.e., stereographic and orthographic), the azimuthal equidistant transformation has lower scale distortion towards the axial pole of the retina (Borodkin & Thompson, 1992). Given that many specialized features of retinas are found in the central region (cf., e.g., Collin, 2008), we deem azimuthal equidistant plot projection an appropriate tool. To generate the map, we apply a thin plate spline interpolator, with density predicted as a function of the (x, y) sampling location upon the plot projection of the hemisphere. Thin plate splines are widely used to smooth noisy empirical data, with a wide range of applications across disciplines (Wahba, 1990). We chose thin plate spline smoothing for its relatively low number of assumptions, its comparably good performance (Garza-Gisholt et al., 2014) and its convenient application to polar-projected data. While global smoothing techniques produce higher errors than local smoothing, using larger-scale smoothing was effective at representing the general zones of high density. The smoothing parameters, spatial resolution, extrapolation (to the retinal equator), and plot rotation (in degrees) can be controlled by the user.

The resultant fit is used to predict one million points across the fit model (1000 × 1000 pixel matrix), resulting in a circular plot of the heat map; other areas of the pixel matrix are left transparent, as they are not mapped to the hemisphere. Change in cell density

across the retinal surface is visualized as an isodensity contour line (Figure 1B, map for the rockmover wrasse, *N. taeniourus*). Crosses specify positions of the original sampling locations. The optic nerve head and falciform process are superimposed. The retinal topography map of the rockmover wrasse shows a prominent horizontal streak of high cell densities that curves dorsotemporally posterior to the falciform process. Highest densities (approx. 10.4×10^4) are found immediately nasal to the falciform process.

As Garza-Gisholt et al. (2014) emphasized, it is important to consider the effect of varying smoothing parameters. In addition to visual inspection of the fit, we underline the importance of a quantitative assessment. The fit_plots() function provides three standard plots from thin plate spline smoothing (R package Fields; Nychka, Furrer, & Sain, 2014), and includes a plot of the frequency distribution of the model error at each of the sampling locations (Figure 1C). We encourage the user to explore the mean prediction errors and the standard deviations of the error distributions of differently smoothed maps (Figure 2A, B). For the purposes of this contribution, we compared maps against published standards in terms of smoothness and general appearance. Please note that this does not imply that these maps are necessarily accurate; a thorough test of map accuracy is planned for future studies. Settings that produce results aesthetically similar to published retinas will vary from map to map, but we found satisfactory results for low lambda values and second order polynomials (Figure 1B), producing
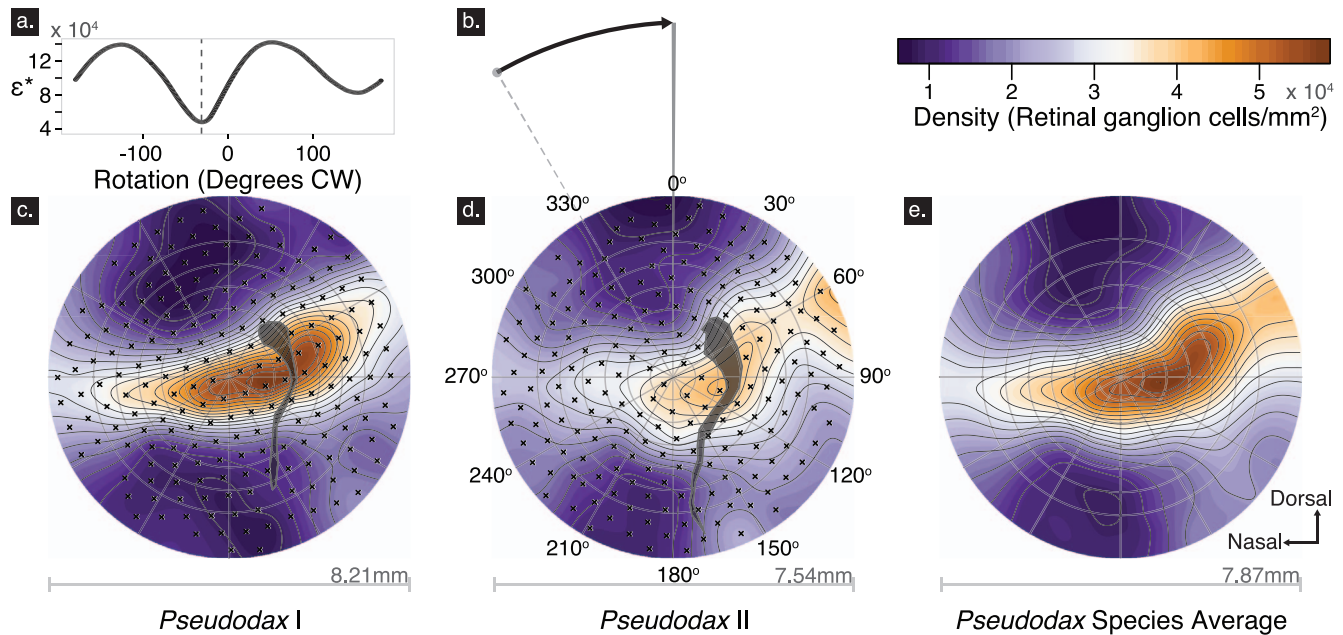
Figure 3. Retina enables the user to compute species average maps. As there is often some uncertainty about the correct anatomical orientation of the samples, the user can enable spin optimization, which helps to overlay maps with minimal orientation error (A; assessed by ε, the absolute mean difference between maps). We determined minimal ε at a 30° rotation (shown in B) of two individual specimens of *Pseudodax moluccanus* (C and D). The composite map representing the species average is visualized in (E). Nasal is on the left, dorsal on top.

low standard deviations with errors still in the range of other model fits. Note that maps with very low lambdas appear overfitted (Figure 2C), similar to some reconstructions of simulated data illustrated by Wood (2003), whereas maps with larger lambdas and higher polynomial order can be too simplified, even though the absolute error is less (Figure 2D–F). Overfitting results in many local minima and maxima of cell densities, yet still allows for recognition of the overall pattern of cell distribution. However, oversimplification may lead to a complete loss of any topographic information.

The retinal map plot is designed for optimal viewing by readers who have normal vision, and for those who may be colorblind (Light & Bartlein, 2004). We used dual-gradient colored indices for each discrete density level (Figure 2B), because two color gradients allow for finer resolution. The Vischeck ImageJ plugin (Dougherty & Wade, 2001) was used to choose the most effective color scheme generated with the RColor-Brewer package (Harrower & Brewer, 2003). Orange and purple are purported to be excellent for visibility in data visualization (Light & Bartlein, 2004), and even when maps are photocopied in greyscale, peaks can still be identified with help from the isodensity lines. The number of contour lines, number of color levels, and choice of color palette can be customized with the col_levels, contour_levels, and col_arguments within the retinaplot() function.

Computing averages of multiple maps in Retina

The composite_map() function averages the densities of multiple retinal maps across a common prediction grid of a specified spatial resolution. Passing this matrix to the plot_from_MAT() function will display an average retinal map, illustrated for two retinas of the chiseltooth wrasse, *P. moluccanus* (Figure 3). The correct anatomical orientation of individual retinal topography maps is essential for correct computation of average maps. However, we have built in a function to account for some uncertainty in anatomical orientation, assuming that the topographic distribution of cells is similar across different individuals. Given that it is sometimes difficult to keep track of the perfect anatomical orientation of a sample, this tool may be helpful. If there is such uncertainty regarding the anatomically correct orientation of the samples, one can enable spin optimization, which can help users overlay maps with minimal orientation error. Essentially, this function aims to align topographic landmarks across different retinas. After the user specifies one retinal map to be "fixed," all other maps are rotated incrementally, and a comparison of the surface difference is recorded for each rotation step. We interpolate both retinas in their new orientation, predict densities on a common grid, and calculate the absolute mean difference between the maps at that spin value (Figure 3A–D). Rotation based on the cell

Input data from any stereology program

Cell counts
Retinal outline
Falciform process/optic disc

xyz.csv
outline.roi
falc.txt

Retistruct reconstructs the retinal hemisphere- sampling points and the falciform process are mapped to spherical coordinates.

Key functionality of retina

Make a retinal map	Combine N maps into a species average
Compute fit statistics for density smoothing	Generate maps with differing smoothing parameters
Compute descriptive statistics and plots for cell-count data	Quickly align and prepare N retinas

How retina makes a map

Optional orientation correction via spin optimization

Projection (azimuthal equidistant) onto flat surface

Fit thin plate spline smoothing function to cartesian data

Color each image pixel by predicting the retinal density from the spline

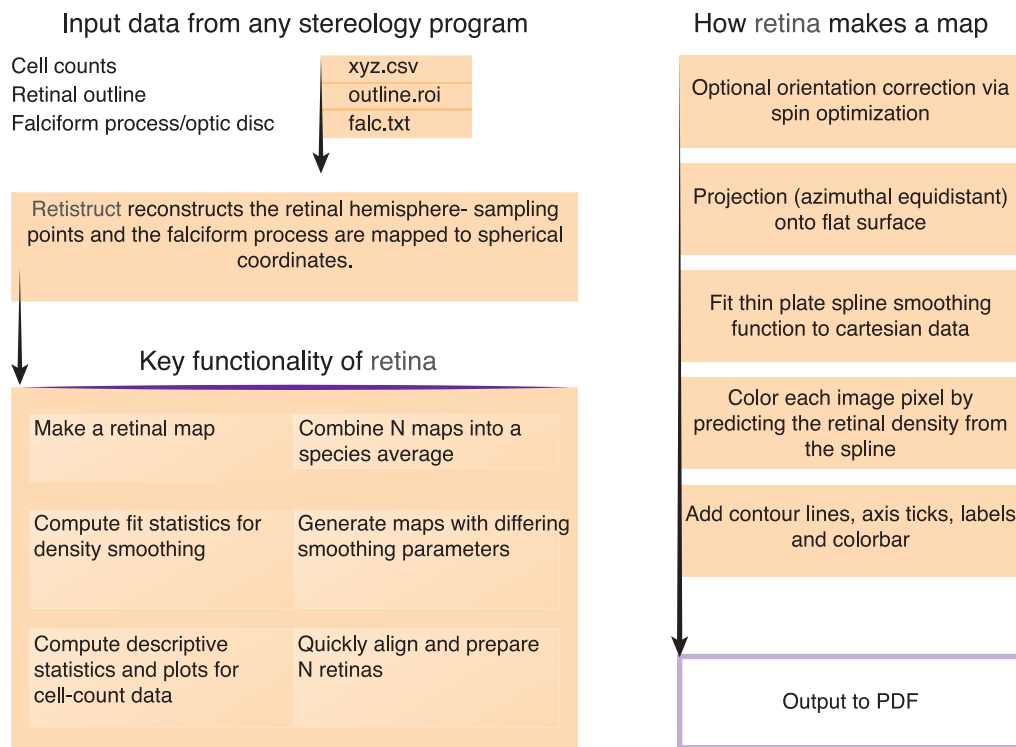Add contour lines, axis ticks, labels and colorbar

Output to PDF

Figure 4. The workflow and functionality of Retina summarized in a flowchart diagram. The left side shows what input data are needed, the role of Retistruct, and the main functionalities of Retina, whereas the right side illustrates the conceptual approach to map illustrations in Retina.

densities did a remarkably good job at lining up the retinas (as suggested by the oriented falciform processes); however, this technique must be very carefully monitored to make sure the orientation chooses reasonable spin optima when minimizing the difference between maps. The underlying assumption that topographic features across retinas of different individuals are consistent should also be verified.

The average map of the chiseltooth wrasse (Figure 3E) does not contain a combined optic nerve head or falciform process. Given that we do not explore species averages of falciform processes in this paper and the original sampling location points are not visible on the species average, the points from both individuals are combined by their interpolations and not by matching sampling sites. Peak cell densities found in the chiseltooth wrasse (up to about 9.76×10^4) are slightly lower than in the rockmover wrasse. Overall, the horizontal streak appears weakly defined, in particular in the nasal parts of the retina.

Discussion

We provide an open source tool that generates retinal topography maps. With Retina, we address some problems that may have hindered a potentially more objective, quantitative, and quicker approach to comparisons of retinal topography. Retina is a tool for the illustration of cell populations across wholemounts, developed on the basis of state-of-the-art techniques. We hope that Retina will not only be useful for visualization purposes, but that it also stimulates additional research in the area of retinal topography mapping. An overview of the workflow and functionality of Retina is depicted in Figure 4.

Several potential sources of error can be identified and warrant further research. Problems with staining and cell identification aside, we identify three main aspects that may require more investigation: the reconstruction of the retinal hemisphere, the two-dimensional projection of retinal data, and the interpolation or smoothing of cell counts.

Reconstruction of the retinal hemisphere

The flattening and incisions of retinal wholemounts have traditionally posed the biggest challenge in retinal mapping. The most complete attempt to solve the deformation issue has been undertaken by Sterratt et al. (2013). Sterratt's approach is more flexible than Curcio's (1989) method, in that it does not require a specific type of incision pattern on the retina. Even though difficult to carry out, initial accuracy estimates

of the reconstruction process are very encouraging. Sterratt et al. (2013) found minimal reconstruction error when locating the position of the optic disk. In particular, additional work on testing the reconstruction accuracy is desirable for work focused on more peripheral locations in the retina.

While resultant maps are expected to be largely devoid of the deformation problem by using Sterratt and colleagues' Retistruct package, there is an assumption of a spherical eye. Although the retina could have been modeled with an ellipsoid representing the original shape of the eye, Sterratt et al. (2013) identified only minimal improvement in model accuracy with the incorporation of rim angle to the reconstruction algorithm. Nevertheless, it may be worthwhile to explore this issue further, especially in light of the shape diversity of the vertebrate eye (e.g., Hall, Kamilar, & Kirk, 2012; Schmitz & Motani, 2010; Schmitz & Wainwright, 2011).

Two-dimensional projection of retinal data

Similar to real topographic data, cell count distributions in retinas can be very complex. Topographic reconstructions in a three-dimensional space are theoretically possible but not necessarily conducive for easy observation or evaluation. Map projections are a user-friendly approach, and there are many different available techniques. We follow the approach by Curcio et al. (1989) and apply an azimuthal equidistant projection, although the projection can be changed by carefully passing a different polar projection specification to both of the composite_map and rotation_optimize functions (McIlroy et al., 2014).

Interpolation or smoothing of cell counts

Possible errors may also result from the illustration of count data. Here, we follow the approach of Curcio et al. (1989) who first projected retinal data into the plane and then performed smoothing. Smoothing is theoretically possible on the scale of the entire hemisphere, but considering the dense sampling site coverage and the small intersampling site distances, we expect errors to be very small.

There are several possible approaches to visualize retinal cell count data, many of which have been applied previously (see Garza-Gisholt et al. (2014) for an overview). Retina produces maps that are based on thin plate splines, a well-established linear smoothing technique (Nychka et al., 2014). Several diagnostic plots make it easy to inspect the model fit, which is important for identifying possible mapping mistakes. Alterations of the smoothing parameters can substan-

tially change the density landscape, and we recommend careful exploration of parameter effects. For example, excessive smoothing may result in missing the presence of a horizontal streak, which seems characteristic of many reef teleosts, including the blue tusk fish *Choerodon albigena* (Labridae; Collin & Pettigrew, 1988). We encourage researchers to include all data (stereology parameters, raw counts, image of sampling grid over wholemount outline) alongside the smoothing parameters so that results can be reproduced and investigated further.

We emphasize that more quantitative data are needed to fully understand what gradients are biologically relevant. This could be approached by selecting random lines across the retina, and sampling densities along those transects. If biologically feasible slopes can be identified, one can force smoothing models to train under the constraint that they cannot change too quickly across a given distance.

While representations of RGC density are sometimes reduced to unidimensional peak and average density measurements, it is important that retinal structure is analyzed as a spatially complex system. Moore et al. (2012) proposed quantitative descriptors of retinal cell topographies, which are helpful in characterizing differences across species. That said, a rigorous quantitative description of maps can only be trusted if the topographic model of cell distributions is reliable.

Conclusions

Retina helps visual ecologists produce visualizations of the distribution of cells across retinal wholemounts. Advantages of Retina include the open source nature of the code that allows easy access for future modifications, the flexibility in reconstructing retinal cell topographies, and the possibility to compute average maps of multiple individuals per species. Easy parameter settings and access to several diagnostic tools simplify the exploration of the influence of smoothing parameters on topographic reconstructions, which is expected to enhance the overall quality of the maps. We hope that Retina opens up further opportunities for quantitative comparative analyses of retinal topography maps.

Keywords: retinal topography maps, visual ecology, retinal ganglion cells, Retistruct, retinal wholemount, retinal flatmount, thin plate spline, visualization

Commercial relationships: none.
Corresponding author: Lars Schmitz.
Email: lschmitz@kecksci.claremont.edu.
Address: W.M. Keck Science Department, Claremont McKenna, Pitzer, and Scripps Colleges, Claremont, CA, USA.

References

Abràmoff, M. D., Magalhães, P. J., & Ram, S. J. (2004). Image processing with ImageJ. *Biophotonics International, 11,* 36–42.

Ahnelt, P. K., Schubert, C., Kübber-Heiss, A., Schiviz, A., & Anger, E. (2006). Independent variation of retinal S and M cone photoreceptor topographies: A survey of four families of mammals. *Visual Neuroscience, 23,* 429–435.

Borodkin, M. J., & Thompson, J. T. (1992). Retinal cartography. An analysis of two-dimensional and three-dimensional mapping of the retina. *Retina, 12,* 273–280.

Bugayevskiy, L. M., & Snyder, J. P. (2002). *Map projections: A reference manual*. Philadelphia, PA: Taylor & Francis Ltd.

Chelvanayagam, D. K. (2000). Interpreting the distortion associated with a retinal wholemount. *Journal of Theoretical Biology, 205,* 443–455.

Chievitz, J. H. (1889). Untersuchungen über die Area centralis retinae. *Archiv für Anatomie und Physiologie*. 139–196.

Coimbra, J. P., Collin, S. P., & Hart, N. S. (2013). Scene from above: Retinal ganglion cell topography and spatial resolving power in the giraffe (*Giraffa camelopardalis*). *Journal of Comparative Neurology, 521*(9), 2042–2057.

Coimbra, J. P., Collin, S. P., & Hart, N. S. (2014a). Topographic specializations in the retinal ganglion cell layer of Australian passerines. *Journal of Comparative Neurology, 522,* 3363–3385.

Coimbra, J. P., Collin, S. P., and Hart, N. S. (2014b). Topographic specializations in the retinal ganglion

cell layer correlate with lateralized visual behavior, ecology and evolution in cockatoos. *Journal of Comparative Neurology, 522,* 3363–3385.

Coimbra, J. P., Nolan, P. M., Collin, S. P., & Hart, N. S. (2012). Retinal ganglion cell topography and spatial resolving power in penguins. *Brain, Behavior and Evolution, 80,* 254–268.

Collin, S. P. (2008). A web-based archive for topographic maps of retinal cell distribution in vertebrates. *Clinical and Experimental Optometry, 91,* 85–95.

Collin, S. P., & Pettigrew, J. D. (1988). Retinal topography in reef teleosts. II. Some species with prominent horizontal streaks and high-density areae. *Brain, Behavior and Evolution, 31,* 283–295.

Collin, S. P., & Pettigrew, J. D. (1989). Quantitative comparison of the limits of visual spatial resolution set by the ganglion cell layer in twelve species of reef teleosts. *Brain, Behavior and Evolution, 34,* 184–192.

Curcio, C. A., Sloan, K. R., & Meyers, D. (1989). Computer methods for sampling, reconstruction, display, and analysis of retinal whole mounts. *Vision Research, 29,* 529–540.

Dougherty, B., & Wade, A. (2001). VisCheck. Retrieved from http://www.vischeck.com/. Accessed 18 June 2014.

Fileta, J. B., Huang, W., Kwon, G. P., Filippopoulos, T., Ben, Y., Dobberfuhl, A., & Grosskreutz, C. L. (2008). Efficient estimation of retinal ganglion cell number: A stereological approach. *Journal of Neuroscience Methods, 170,* 1–8.

Frisén, L. (1970). The cartographic deformations of the visual field. *Ophthalmologica, 161,* 38–54.

Garza-Gisholt, E., Hemmi, J. M., Hart, N. S., & Collin, S. P. (2014). A comparison of spatial analysis methods for the construction of topographic maps of retinal cell density. *PLoS One, 9,* e93485.

Hall, M. I., Kamilar, E. C., & Kirk, E. C. (2012). Eye shape and the nocturnal bottleneck of mammals. *Proceedings of the Royal Society B: Biological Sciences, 279,* 4962–4968.

Harrower, M., & Brewer, C. A. (2003). ColorBrewer. org: An online tool for selecting colour schemes for maps. *The Cartographic Journal, 40,* 27–37.

Landgren, E., Fritsches, K., Brill, R., & Warrant, E. (2014). The visual ecology of a deep-sea fish, the escolar *Lepidocybium flavobrunneum* (Smith, 1843). *Philosophical Transactions of the Royal Society B, 369,* 20130039.

Light, A., & Bartlein, P. J. (2004). The end of the rainbow? Color schemes for improved data graphics. *EOS, 85,* 385–391.

Lisney, T. J., Stecyk, K., Kolominsky, J., Graves, G. R., Wylie, D. R., & Iwaniuk, A. N. (2013). Comparison of eye morphology and retinal topography in two species of new world vultures (Aves: Cathartidae). *Anatomical Record, 296,* 1954–1970.

Lisney, T. J., Stecyk, K., Kolominsky, J., Schmidt, B. K., Corfield, J. R., Iwaniuk, A. N., & Wylie, D. R. (2013). Ecomorphology of eye shape and retinal topography in waterfowl (Aves: Anseriformes: Anatidae) with different foraging modes. *Journal of Comparative Physiology A, 199,* 385–402.

Mass, A. M., & Supin, Y. (1989). Distribution of ganglion cells in the retina of an Amazon river dolphin *Inia geoffrensis. Aquatic Mammals, 15*(2), 49–56.

McIlroy, D. (2014). mapproj: Map Projections. R package version 1.2-2. Packaged for R by R. Brownrigg, T. P. Minka; transition to Plan 9 codebase by R. Bivand. Retrieved from http://CRAN.R-project.org/package=mapproj

Moore, B. A., Doppler, M., Young, J. E., & Fernández-Juricic, E. (2013). Interspecific differences in the visual system and scanning behavior of three forest passerines that form heterospecific flocks. *Journal of Comparative Physiology A, 199,* 263–277.

Moore, B. A., Kamilar, J. M., Collin, S. P., Bininda-Emonds, O. R. P., Dominy, N. J., Hall, M. I. . . . Fernández-Juricic, E. (2012). A novel method for comparative analysis of retinal specialization traits from topographic maps. *Journal of Vision, 12*(12): 13, 1–24, doi:10.1167/12.12.13. [PubMed] [Article]

Newman, A. S., Marshall, J. N., & Collin, S. P. (2013). Visual eyes: A quantitative analysis of the photoreceptor layer in deep-sea sharks. *Brain, Behavior and Evolution, 82,* 237–249.

Nychka, D., Furrer, R., & Sain, S. (2014). Fields: Tools for spatial data. R package version 7.1. Retrieved from http://CRAN.R-project.org/package=fields

R Development Core Team. (2014). *R: A language and environment for statistical computing.* Vienna, Austria: R Foundation for Statistical Computing. Retrieved from http://www.R-project.org/

Schiviz, A. N., Ruf, T., Kuebber-Heiss, A., Schubert, C., & Ahnelt, P. K. (2008). Retinal cone topography of artiodactyl mammals: Influence of body height and habitat. *Journal of Comparative Neurology, 507,* 1336–1350.

Schmitz, L., & Motani, R. (2010). Morphological differences between the eyeballs of nocturnal and diurnal amniotes revisited from optical perspectives of visual environments. *Vision Research, 50,* 936–946.

Schmitz, L., & Wainwright, P. C. (2011). Nocturnality constrains morphological and functional diversity in the eyes of reef fishes. *BMC Evolutionary Biology, 11,* 338.

Shapley, R., & Perry, V. H. (1986). Cat and monkey retinal ganglion cells and their visual functional roles. *Trends in Neurosciences, 9,* 229–235.

Snyder, J. P. (1987). *Map projections: A working manual.* USGS Professional Paper No. 1395. http://pubs.er.usgs.gov/publication/pp1395

Sterratt, D. C., Lyngholm, D., Willshaw, D. J., & Thompson, I.D. (2013). Standard anatomical and visual space for the mouse retina: Computational reconstruction and transformation of flattened retinae with the Retistruct package. *PLoS Computational Biology, 9,* e1002921.

Stone, J. (1965). A quantitative analysis of the distribution of ganglion cells in the cat's retina. *Journal of Comparative Neurology, 124,* 337–352.

Stone, J. (1981). *The whole mount handbook: a guide to the preparation and analysis of retinal whole mounts.* Sydney, Australia: Maitland Publications.

Stone, J., Rapaport, D. H., Williams, R. W., & Chalupa, L. (1981). Uniformity of cell distribution in the ganglion cell layer of prenatal cat retina: Implications for mechanisms of retinal development. *Developmental Brain Research, 2,* 231–242.

Temple, S. E., Manietta, D., & Collin, S. P. (2013). A comparison of behavioural (Landolt C) and anatomical estimates of visual acuity in archerfish (*Toxotes chatareus*). *Vision Research, 83,* 1–8.

Ullmann, J. F. P., Moore, B. A., Temple, S. E., Fernández-Juricic, E., & Collin, S. P. (2012). The retinal wholemount technique: A window to understanding the brain and behaviour. *Brain, Behavior and Evolution, 79,* 26–44.

von Graefe, A. (1865). Rede über die Bedeutung ophthalmologischer Studien für die Medizin. Zur Feier des ein und siebenzigsten Stiftungstages des medizinisch-chirurgischen Friedrich-Wilhelms-Instituts am 2. August 1865. Berlin, Germany: Verlag von Hermann Peters.

Wahba, G. (1990). *Spline models for observational data.* CBMS-NSF regional conference series in applied mathematics. Philadelphia, PA: Society for Industrial and Applied Mathematics.

West, M. J. (2012). *Basic Stereology for Biologists and Neuroscientists.* Cold Spring Harbor, NY: Cold Spring Harbor Press.

Wood, S. N. (2003). Thin plate regression splines. *Journal of the Royal Statistical Society B, 65,* 95–114.